Role of bubble growth dynamics on microscale heat transfer events in microchannel flow boiling process

Sajjad Bigham, and Saeed Moghaddam

Citation: Appl. Phys. Lett. **107**, 244103 (2015); doi: 10.1063/1.4937568
View online: https://doi.org/10.1063/1.4937568
View Table of Contents: http://aip.scitation.org/toc/apl/107/24
Published by the American Institute of Physics

Role of bubble growth dynamics on microscale heat transfer events in microchannel flow boiling process

Sajjad Bigham and Saeed Moghaddam[a)]
Department of Mechanical and Aerospace Engineering, University of Florida, Gainesville, Florida 32611, USA

(Received 26 May 2015; accepted 29 November 2015; published online 15 December 2015)

For nearly two decades, the microchannel flow boiling heat transfer process has been the subject of numerous studies. A plethora of experimental studies have been conducted to decipher the underlying physics of the process, and different hypotheses have been presented to describe its microscopic details. Despite these efforts, the underlying assumptions of the existing hypothesis have remained largely unexamined. Here, using data at the microscopic level provided by a unique measurement approach, we deconstruct the boiling heat transfer process into a set of basic mechanisms and explain their role in the overall surface heat transfer. We then show how this knowledge allows to relate the bubble growth and flow dynamics to the surface heat flux. © *2015 AIP Publishing LLC*. [http://dx.doi.org/10.1063/1.4937568]

Numerous studies[1–7] have been conducted to understand the physics of the boiling heat transfer process in microchannels in order to better predict and enhance its performance. Despite these efforts, the underlying physics of the process has not yet been elucidated. The main obstacles in achieving this goal are the complex coupling of mass, momentum, and energy transport occurring between different phases, and the difficulty in implementing an adequate measurement tool for resolving the thermal field at small scales.

In the absence of a microscale description of heat transfer events, different and sometimes contradictory hypotheses regarding the mechanisms through which heat is transferred to the fluid[8–13] have been proposed. An in-depth understanding of microscale heat transfer events can only be achieved if new measurement tools are utilized to resolve the thermal field at the solid-fluid interface at sufficiently high spatial and temporal resolutions.

Measurement of the surface heat flux is the main challenge in resolving the thermal field at the solid-fluid interface.[14,15] Surface heat flux at the solid-fluid interface rapidly varies in time and space domains due to bubbles nucleation, expansion, and movement along the channel, which result in the formation and evaporation of thin liquid films with varying thickness, contact line movements, and rapid surface wetting and dryout. As will be shown later in this paper, the heat flux associated with these events can change from zero to its maximum value within less than 100 μs, and regions with maximum and minimum (near zero) heat flux could be only a few micrometers apart. As a result, the individual heat transfer events associated with the boiling sub-processes are coupled through the substrate, as shown in the experimental studies of Yabuki and Nakabeppu[16] and Rao *et al.*[17] This coupling between the heat transfer events makes the measurements challenging, since the heat flux assocaited with the individual sub-processes cannot be accurately measured.

In the absence of a viable approach for accurate measurement of the surface heat flux, different strategies have been implemented to determine the surface heat flux. Attempts have been made to subject the heated surface to a constant heat flux,[18] to numerically calculate the surface flux by solving the thermal field within the solid using experimental surface temperature data,[16,19,20] and to electronically vary the heat flux across a micro-heater array such that the surface temperature always remains constant.[21] Notably, in an effort to decouple the boiling sub-processes, Demiray and Kim[21] maintained a constant temperature over the surface and utilized a low thermal conductivity (low-k) substrate. However, the main difficulty with this approach is that the heat loss through the substrate could be several times greater than the surface-to-liquid heat flux.[22]

Here, a composite wall that consists of a high thermal conductivity silicon (Si) substrate coated by a thin layer of a low-k polymer (SU8) is utilized. Temperature sensors are embedded within the wall. This arrangement of materials and sensors, originally introduced by Moghaddam and Kiger,[23,24] allows to overcome the difficulties associated with resolving the surface heat flux. In the boiling of dielectric liquids, the surface temperature at the silicon-polymer interface remains at a relatively constant temperature due to the high thermal conductivity of the Si substrate. Under these conditions, any change in the surface heat flux directly changes the temperature at the top of the polymer layer. In addition, since the polymer layer is very thin and has a low thermal conductivity, its lateral heat conduction is quite small. Using the known temperature boundary conditions across the polymer, transient heat conduction within the polymer layer is numerically solved to determine the surface heat flux.

A detailed view of the test article is provided in Fig. 1. A total of 53 platinum resistance temperature detectors (RTDs) are fabricated at the silicon-SU8 and SU8-fluid interfaces. The RTDs are 50-μm-wide and are spaced 15 μm apart in the flow direction (cf. Fig. 1(b)). A single microchannel with a rectangular cross-section made of a 75-μm-thick SU8 film is then spun-coated on the sensor array. The microchannel width is 300 μm. The channel is then capped by an optically

a)Email: saeedmog@ufl.edu

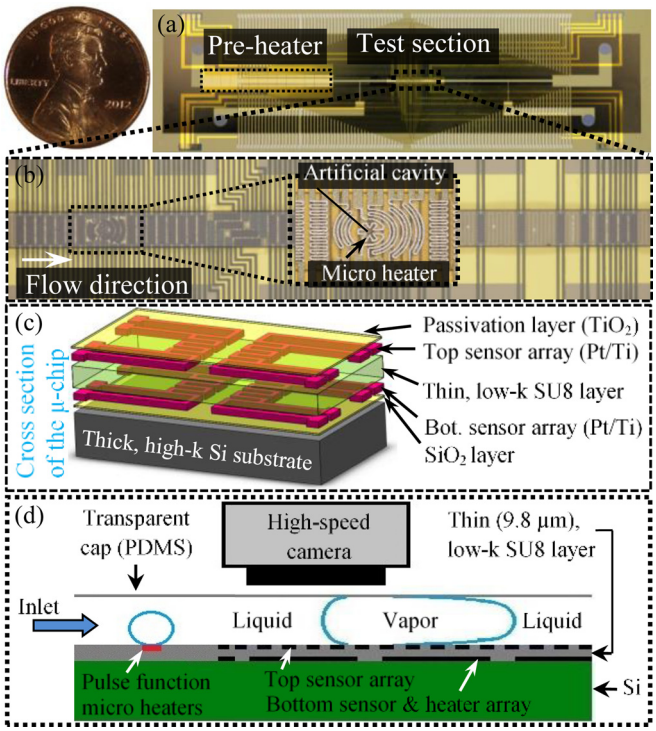

FIG. 1. (a) An image of the microfluidic chip (pre-heater and test sections are labeled); (b) a close view of the test section (inset shows a zoomed view of the pulsed function microheater); (c) a schematic view of the composite substrate cross-section; and (d) a schematic of the experimental device.

transparent Polydimethylsiloxane (PDMS) cap (cf. Fig. 1(d)). The chip is equipped with a pre-heater section made to heat up the working fluid (FC-72) to a desired temperature before entering the test section (cf. Fig. 1(a)). To control the nucleation site, a 300 nm in diameter cavity is fabricated using a focused ion beam (FIB) milling machine. The cavity is surrounded by a pulsed function microheater fabricated on the SU8 film (cf. Fig. 1(b)). Changing the amplitude and period of the pulsed function microheater subjects the liquid mass near the cavity to different metastable superheated conditions (i.e., non-equilibrium thermodynamic conditions) generating different flow regimes.[25] Since the total surface covered by the microheater is quite small ($\sim$0.004 mm^2), the overall heat gain by the liquid is negligible. The temperature data and the synchronized bubble images are recorded at a frequency of 20 kHz. Details of the fabrication process, experimental procedures, calibration tests, and uncertainty analysis are presented in the supplementary material.[26]

Using the unprecedented measurement capabilities enabled by the experimental platform discussed above, some of the long-standing questions concerning the magnitude and time period of activation of different mechanisms of heat transfer and their relations to dynamics of the bubble growth and flow through the microchannel can be studied. The following sections provide example data at limited test conditions to illustrate how the bubbles growth and flow process triggers different surface heat transfer events.

The images of a moving bubble during its growth and the corresponding local temperature data measured at a downstream sensor are shown in Figs. 2(a) and 2(b). The blue and red shadow lines indicate the time at which the front and rear sides of the bubble arrive at the sensor. As it can be seen, the bubble passing time over the sensor, τ, is 14 ms. The corresponding local heat flux-time history is shown in Fig. 2(c). The heat flux variations starts by a heat flux spike up to about 10–12 W/cm^2 when the front side of the bubble moves over the sensor footprint. Therefore, the observed heat flux spike is due to phase change cooling resulting from microlayer and/or interline evaporation modes of heat transfer. After a while, the local heat flux declines and reaches a partial dryout stage with a low heat flux. The decreasing trend in the local heat flux can be explained upon examination of the bubble images, where it can be observed that the liquid film located between the vapor region and the channel sidewalls is evaporated/disappeared. Therefore, liquid shortage results in a gradual decline in the local heat flux. Toward the end of the partial dryout process, the local heat flux rapidly increases as the rear end of the bubble rewets the sensor footprint. This sudden spike in the local heat flux resembles observations made in pool boiling studies[18,20,27] during the bubble departure, as a liquid front advances over (i.e., rewets) the bubble-surface contact area after a dryout period following the microlayer evaporation process. The physics of this process is consistent with what is commonly named as "transient conduction" mode of heat transfer, which results from the rewetting of a hot surface with the cooler bulk liquid.

After the liquid slug fully rewets the surface, the local heat flux gradually decreases and reaches a steady state condition. Using the surface temperature and the liquid saturation temperature, the Nu number is determined to be 8.9. Section S4 of the supplementary material[26] provides an experimental study on single-phase Nu number and its comparison with an analytical solution. Comparison of the Nu number associated with the liquid slug flow in the channel with that of the single phase flow (Nu = 5.4) shows a 65% enhancement in heat transfer. Therefore, hereafter, we refer to this mechanism of heat transfer as the single-phase convection heat transfer mode. The data clearly show that the thin film evaporation mechanism is the most effective mode of heat transfer compared to the other mechanisms of heat transfer. Using an energy balance approach (details are provided in S7), the liquid film thickness for the bubble presented in Fig. 2(a) is determined to be 4.6 μm.

The timespan of each heat transfer event varies with the bubble length. The results indicated that as the length of the bubble decreases, first, the dryout region diminishes, and then the thin film evaporation and the transient conduction heat transfer modes start diminishing. Fig. 2(d) shows the heat flux data at a sensor that has experienced a shorter bubble with a passing time of $\tau = 5.3$ ms over a sensor. The actual images of a bubble and the corresponding surface temperature data are reported in the supplementary material (cf. Figs. S9).[26] The results clearly indicate the absence of a dryout event. Consistent with the observations discussed earlier, the surface heat flux spikes as a result of the microlayer/interline evaporation mechanism of heat transfer as soon as the bubble moves over the sensor. However, the rear end of the bubble arrives at the sensor before the microlayer fully evaporates, resulting in truncation of the thin film evaporation heat transfer regime. Consequently, the thin film evaporation and the transient conduction processes appear as a single heat transfer event. Fig. 2(e) shows the heat flux associated with

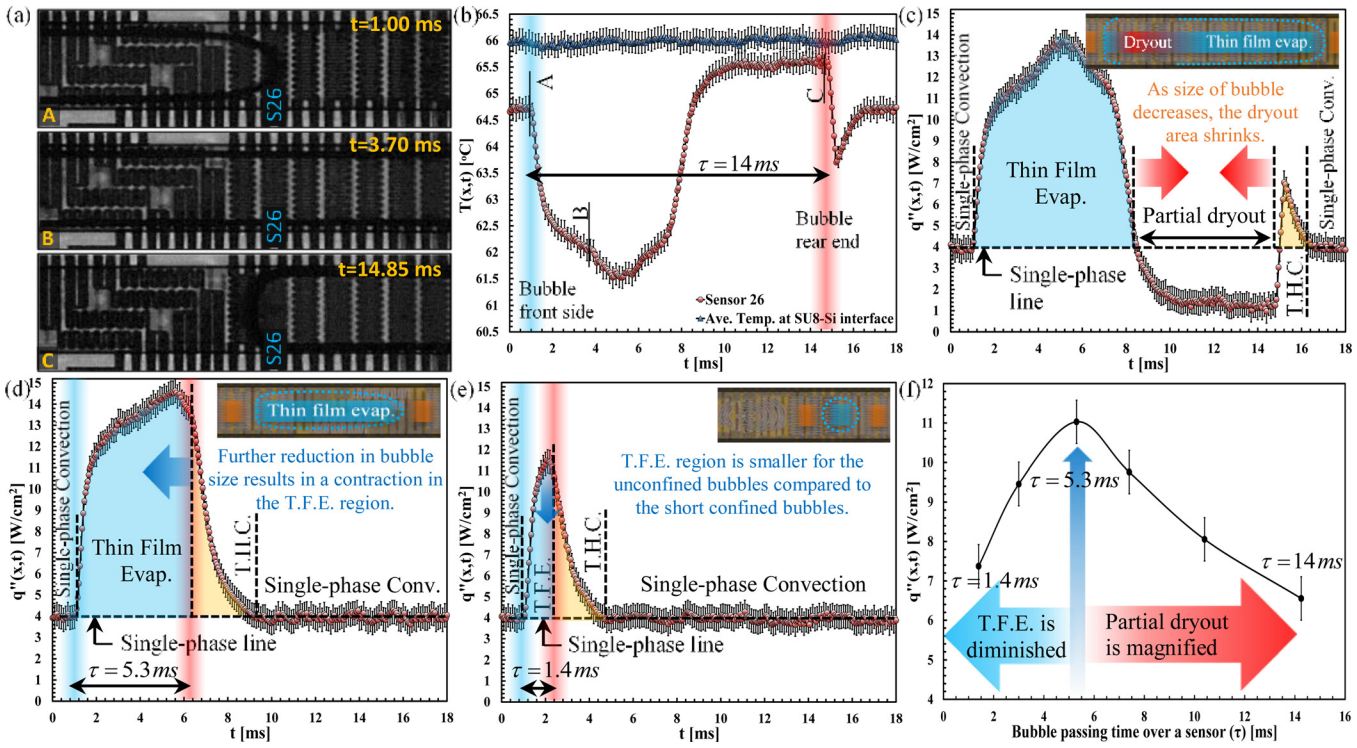

FIG. 2. (a) Images; (b) temperature-time histories; and (c) local heat flux-time histories corresponding to a bubble with a passing time of $\tau = 14$ ms. (d) and (e) Local heat flux-time histories corresponding to bubbles with passing times of $\tau = 5.3$ ms and $\tau = 1.4$ ms, respectively. Average surface heat fluxes as a function of a bubble passing time over a sensor is shown in (f). T.H.C. stands for transient heat conduction.

the bubble at its early growth stage, where the microlayer evaporation heat transfer event is truncated quite early, resulting in a significant decline in the surface heat flux.

The data discussed above clearly suggest that there must exists a bubble size at which the surface heat flux at a target location is maximal. To verify this assumption, we analyzed the heat transfer data over a set of sensors that have experienced the bubble at different lengths (cf. Fig. 2(f)). Let us assume that the liquid and vapor phases are traveling at a velocity of U to estimate the bubble length L ($\sim U\tau$) for a given sensor and bubble pair. The results clearly indicated that the bubble has experienced the maximum heat flux at a passing time of 5.3 ms (or $L \sim 11\ D_h$). The thin film evaporation event truncated early for shorter bubbles ($L \lesssim 11\ D_h$) before this effective mechanism of heat transfer could significantly contribute to the overall surface flux, and longer bubbles ($L \gtrsim 11\ D_h$) experienced partial dryout, thus reducing the overall heat transfer.

Table I provides a detailed breakdown of the magnitude of all heat transfer mechanisms and their relative contributions during one cyclic passing of a liquid slug, an elongated bubble, and a partial dryout region (if it exists). A comparison of the data of bubbles at $\tau = 5.3$ ms and $\tau = 10.4$ ms suggests that the maximum heat flux occurs when the contribution of the microlayer evaporation mechanism maximizes while the surface does not experience partial dryout. At $\tau = 5.3$ ms, the microlayer evaporation process is responsible for 54% of the overall surface heat transfer, while the transient conduction and single-phase convection processes have moderate contributions. At $\tau = 10.4$ ms, surface heat flux due to microlayer evaporation is higher than that of the other mechanisms, but the transient conduction and single-phase convection heat transfer mechanisms make little contributions to the overall surface heat flux. Detailed information of the individual heat transfer events at different mass flow rates and heat fluxes are reported in the supplementary material.[26]

In conjunction with an optimal bubble length that maximizes the surface heat flux at a target location, there is a bubble frequency at which the heat flux at the target location

TABLE I. A detailed breakdown of the magnitude of all heat transfer mechanisms and their relative contributions. T.F.E., T.H.C., and S.P.C. stand for thin film evaporation, transient heat conduction, and single-phase convection, respectively.

		Surface heat transfer (μJ)				% contribution of heat transfer mechanisms			
τ (ms)	L/D_h	T.F.E.	T.H.C.	Partial dryout	S.P.C.	T.F.E.	T.H.C.	Partial Dryout	S.P.C.
1.4	2.9	2.2	2.3	…	9.3	16	17	…	67
3	6.3	5.7	3	…	8.1	34	18	…	48
$\tau_{opt} = 5.3$	11	11.2	3	…	6.5	54	14	…	32
7.4	15.4	13.6	1.3	0.3	5.6	65	6	1	28
10.4	21.7	13.6	1.3	0.9	3.9	69	7	5	19

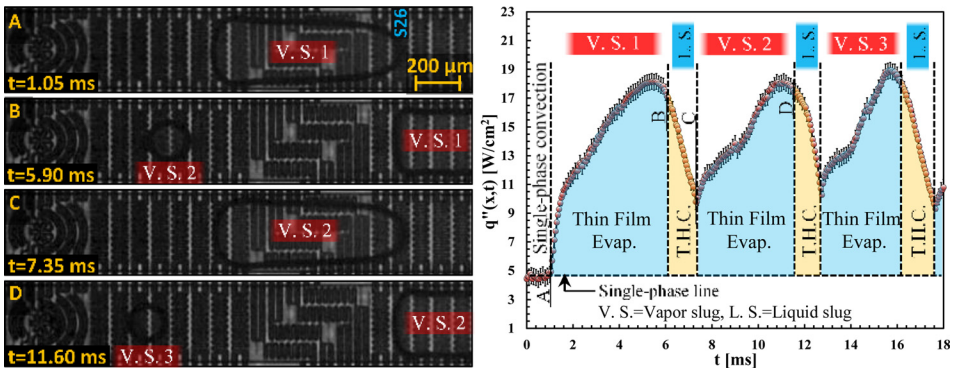

FIG. 3. Consecutive thin film evaporation and transient heat conduction heat transfer events occurring over a sensor footprint at a mass flux of 93.3 kg/m^2-s.

peaks. This conclusion takes into consideration the fact that single-phase convection is the least efficient heat transfer mechanism, and the transient conduction mechanism only rivals the thin film evaporation mechanism for a very short period of time before it rapidly declines. It is evident that the heat flux can be maximized if both of these relatively less efficient mechanisms of heat transfer are circumvented. To achieve this objective, the bubble generation rate is increased in steps by adjusting the frequency of the voltage signal applied to the microheater surrounding the cavity.

The optimal bubble generation frequency can be estimated by the reciprocal of the bubble passing time at its optimal length ($1/\tau_{opt}$). At a mass flux of 93.3 kg/m^2-s with $\tau_{opt} = 4.6$ ms, the optimal bubble generation frequency is almost 217 bubbles/s (cf. Table S1 of the supplementary material[26]). Fig. 3 provides the results of a test conducted close to the optimal bubble generation frequency at approximately 190 bubbles/s. As the results suggest, the single-phase convection mechanism is readily circumvented, but the transient conduction mode is still partially present. The tests suggested that a quick transition to annular flow takes place when the length of the liquid slug is significantly reduced. The liquid slug preceding a bubble feeds the microlayer, since the bubble slides over a layer of liquid adjacent to the wall as it moves along the channel. Perhaps the duration of the transient conduction process could be further reduced by decreasing the liquid slug length. Given the fact that a more precise control of the events is difficult, and a transition between slug and annular flow occurs quite rapidly, the data shown in Fig. 3 present a near optimal heat flux at the target location.

A comparison of the data presented in Tables I and S1 reveals that τ_{opt} decreases as the mass flow rate increases. This can be attributed to the thickness of the initial liquid layer laid down by the liquid slug, which decreases as the liquid slug travels at higher velocities. The thinner the initial liquid layer thickness, the faster it evaporates (i.e. lower τ_{opt}). As a result, the optimal bubble generation frequency increases at higher mass flow rates. In addition, a comparison of the data shown in Tables I and S2 indicates that τ_{opt} decreases as the heat flux increases. This is because the initial liquid layer laid down by the liquid slug evaporates faster at higher heat fluxes, thus reducing τ_{opt}. Consequently, the optimal bubble generation frequency increases as the applied heat flux increases.

In summary, we reported microscale details of the heat transfer events during the evolution of a bubble in flow boiling of FC-72 in a microchannel. The thermal field at the fluid-solid interface was resolved at a spatial resolution of 40–65 μm and a temporal resolution of 50 μs. The magnitude, time period of activation, and relative contributions of different boiling sub-processes were determined relative to the bubbles' growth stages. It was determined that properties of the boiling sub-processes depend on the bubble growth dynamics. The bubble size at which the average surface heat flux at a target location reaches a maximum value was determined. It was experimentally determined that the thin film evaporation mode of heat transfer is the most effective heat transfer sub-process in flow boiling in a microchannel. To extend the time period of activation of this effective mode of heat transfer, the waiting time between successive bubbles was carefully tailored. It was shown that understanding the microscopic details of the heat transfer events can help dissect the boiling process and implement its more effective sub-processes. These data can serve as validation benchmarks and allow fine-tuning of the microchannel flow boiling heat transfer models.

This study was supported by a grant from the National Science Foundation (NSF) under Contract No. CBET-1403657. Fabrication of the devices was conducted in the Nanoscale Research Facility (NRF) at the University of Florida.

[1]S. G. Kandlikar, J. Heat Transfer **134**, 034001 (2012).
[2]S.-M. Kim and I. Mudawar, Int. J. Heat Mass Transfer **77**, 627 (2014).
[3]S. Szczukiewicz, M. Magnini, and J. R. Thome, Int. J. Multiphase Flow **59**, 84 (2014).
[4]J. R. Thome, Int. J. Heat Fluid Flow **25**, 128 (2004).
[5]S. R. Rao and Y. Peles, Int. J. Heat Mass Trans. **89**, 482–493 (2015).
[6]T. Harirchian and S. V. Garimella, Int. J. Multiphase Flow **35**(4), 349–362 (2009).
[7]D. Li and V. K. Dhir, J. Heat Transfer **129**(7), 864–876 (2007).
[8]M. W. Wambsganss, D. M. France, J. A. Jendraejczyk, and T. N. Tran, J. Heat Transfer **115**, 963 (1993).
[9]T. N. Tran, M. W. Wambsganss, and D. M. France, Int. J. Multiphase Flow **22**, 485 (1996).
[10]J. R. Baird, Z. Y. Bao, D. F. Fletcher, and B. S. Haynes, in *Proceedings of the Boiling 2000 Phenoena and Emerging Applications, Anchorage, Alaska, 30 April–5 May 2000*, pp. 447–466.
[11]S. G. Kandlikar and P. Balasubramanian, Heat Transfer Eng. **25**, 86 (2004).
[12]Y. Y. Yan and T. F. Lin, Int. J. Heat Mass Transfer **41**, 4183 (1998).
[13]W. Qu and I. Mudawar, Int. J. Heat Mass Transfer **46**, 2755 (2003).
[14]S. Bigham and S. Moghaddam, Int. J. Heat Mass Trans. **88**, 111–121 (2015).
[15]S. Bigham and S. Moghaddam, in *Proceedings of ASME 2015 International Technical Conference and Exhibition on Packaging and Integration of Electronic and Photonic Microsystems (InterPACK2015)*

and the International Conference on Nanochannels, Microchannels and Minichannels (ICNMM2015) (San Francisco, California, July 6–9, 2015), Paper No. IPACK2015-48581, pp. V002T06A017.
[16]T. Yabuki and O. Nakabeppu, in *Proceedings of the 14th International Heat Transfer Conference IHTC14, Washington DC, USA, 8–13 August 2010*, pp. 1–7.
[17]S. R. Rao, F. Houshmand, and Y. Peles, Int. J. Heat Mass Transfer **76**, 317 (2014).
[18]L. Zhang, J. Koo, L. Jiang, M. Asheghi, K. E. Goodson, J. G. Santiago *et al*., J. Microelectromech. Syst. **11**, 12–19 (2002).
[19]E. Wagner and P. Stephan, J. Heat Transfer **131**, 1210081 (2009).
[20]T. Yabuki and O. Nakabeppu, Int. J. Heat Mass Trans. **76**, 286–297 (2014).
[21]F. Demiray and J. Kim, Int. J. Heat Mass Transfer **47**, 3257 (2004).
[22]S. Moghaddam, "Microscale study of nucleation process in boiling of low-surface-tension liquids," Ph.D. thesis (University of Maryland, College Park, MD, 2006).
[23]S. Moghaddam and K. Kiger, Int. J. Heat Mass Transfer **52**, 1284 (2009).
[24]S. Moghaddam, K. T. Kiger, A. Modafe, and R. Ghodssi, J. Microelectromech. Syst. **16**, 1355 (2007).
[25]V. P. Carey, *Liquid-Vapor Phase Change Phenomena: An Introduction to the Thermophysics of Vaporization and Condensation Processes in Heat Transfer* (Hemisphere Publishing Corporation, 1992).
[26]See supplementary material at http://dx.doi.org/10.1063/1.4937568 for details of the fabrication process, experimental procedure, calibration tests, uncertainty analysis, single phase flow tests, actual images of a bubble, and the corresponding surface temperature data (n.d.).
[27]S. Moghaddam and K. Kiger, Int. J. Heat Mass Transfer **52**, 1295 (2009).